

Exploring the flow harmonic correlations via multi-particle symmetric and asymmetric cumulants in Au+Au collisions at $\sqrt{s_{NN}} = 200$ GeV

Kaiser Shafi,^{*} Prabhupada Dixit,[†] Sandeep Chatterjee,[‡] and Md. Nasim[§]
Indian Institute of Science Education and Research Berhampur
 (Dated: November 19, 2024)

We study multi-particle azimuthal correlations in Au+Au collisions at $\sqrt{s_{NN}} = 200$ GeV. We use initial conditions obtained from a Monte-Carlo Glauber model and evolve them within a viscous relativistic hydrodynamics framework that eventually gives way to a transport model in the late hadronic stage of the evolution. We compute the multi-particle symmetric and asymmetric cumulants and present the results for their sensitivity to the shear and bulk viscosities during the hydrodynamic evolution. We also check their sensitivity to resonance decay and hadronic interactions. We demonstrate that while some of these observables are more sensitive to transport properties than traditional flow observables, others are less sensitive, making them suitable for studying different stages of the evolution.

I. INTRODUCTION

In ultra-relativistic heavy-ion collisions, a thermalized, strongly interacting, deconfined medium, known as Quark-Gluon Plasma (QGP), is expected to form [1–6]. The information regarding certain properties of QGP is carried by anisotropies observed in the momentum distributions of the produced particles [3, 7, 8]. After hadronization, particles are emitted anisotropically in the transverse plane to the beam direction, as detected by a detector. Traditionally, Fourier series in flow amplitudes v_n and symmetry planes ψ_n are used to quantify this azimuthal distribution in the momentum space [9],

$$\frac{dN}{d\phi} = \frac{1}{2\pi} \left[1 + 2 \sum_{n=1}^{\infty} v_n \cos[n(\phi - \psi_n)] \right] \quad (1)$$

Collective flow is crucial for studying the properties of the QGP medium formed in these collisions [7, 10, 11]. The impact parameter driven spatial geometry of the fireball, event-by-event nucleon position as well as sub-nucleonic fluctuations within the overlap region of the two colliding nuclei lead to the development of various orders of anisotropic flow harmonics. Due to the almond shape of the overlap region, the primary source of the second-order flow harmonic, known as elliptic flow (v_2), is the initial spatial anisotropy [12–18]. The third-order flow harmonic, known as triangular flow (v_3), arises from event-by-event fluctuations in the positions of the colliding nucleons as well as their sub-nucleonic fluctuations [19–23]. These fluctuations also give rise to higher-order flow harmonics. Previous studies have demonstrated that these flow harmonics are sensitive to the equation of state (EoS) and the transport properties of the fireball created in the collision, such as shear and bulk viscosity [24–28].

Anisotropic flow analysis involves measuring v_n , ψ_n , and their event-by-event correlations and fluctuations. Due to the random fluctuations of the impact parameter vector, however, the estimation of v_n and ψ_n involves the complications associated with reaction plane dispersion in conventional flow analyses. As a result, they are indirectly estimated using correlation techniques, in which there is no need for an event-by-event determination of the reaction plane [29, 30]. Therefore, there is no need to correct for dispersion in an estimated reaction plane. The foundation of this alternative approach is based on the following outcome,

$$\langle e^{i(n_1\phi_1 + n_2\phi_2 + \dots + n_k\phi_k)} \rangle = v_1 v_2 \dots v_k e^{i(n_1\psi_1 + n_2\psi_2 + \dots + n_k\psi_k)} \quad (2)$$

which analytically relates multiparticle azimuthal correlators and flow degrees of freedom [31]. The average is calculated over all unique sets of k different particles in a single event. This expression can be used to determine the properties of flow amplitudes v_n and symmetry planes ψ_n on an event-by-event basis. Apart from collective flow, other sources of correlations called non-flow are also present that typically involve only a subset of particles.

Multivariate cumulants were introduced in anisotropic flow analyses in the early 2000s in Refs. [32, 33], which tackled long-standing issues in the field and transformed the approach to anisotropic flow analysis in high-energy physics. For example, the four-variate cumulant that is used to estimate the flow amplitude, v_n , from four-particle correlation is defined as [33]

$$c_n\{4\} = \langle \langle e^{in(\phi_1 + \phi_2 - \phi_3 - \phi_4)} \rangle \rangle - 2 \langle \langle e^{in(\phi_1 - \phi_3)} \rangle \rangle^2, \quad (3)$$

The double angular brackets indicate that the averaging procedure is performed in two steps, averaging over all distinct particle multiplets in an event and then averaging these single-event averages with appropriately chosen event weights. By generalizing this concept for non-identical harmonics, new observables, which strictly satisfy all defining mathematical properties of cumulants, were constructed to quantify the correlations among different flow harmonics [34]. Ref. [35] further generalized

^{*} kaisers@iiserbpr.ac.in

[†] prabhupadad@iiserbpr.ac.in

[‡] sandeep@iiserbpr.ac.in

[§] nasim@iiserbpr.ac.in

these observables to probe the genuine correlation between different moments of flow harmonics.

A. Symmetric Cumulants of Flow Amplitudes

Reference [34] proposed a general algorithm to measure multi-particle correlation where the harmonics inside the correlator bracket of Eq. (3) can be different. This introduces a new set of observables, known as symmetric cumulants (*SCs*), which can be used to measure the correlation between event-by-event fluctuation of flow harmonics v_m and v_n . This new approach allows for the separation of non-flow and flow contributions and provides initial insights into how the combinatorial background contributes to flow measurements using correlation techniques. These four-particle symmetric cumulants, $SC(m, n)$, are defined as [36]

$$\begin{aligned} SC(m, n) &\equiv \langle \langle \cos(m\varphi_1 + n\varphi_2 - m\varphi_3 - n\varphi_4) \rangle \rangle_c \\ &= \langle \langle \cos(m\varphi_1 + n\varphi_2 - m\varphi_3 - n\varphi_4) \rangle \rangle \\ &\quad - \langle \langle \cos[m(\varphi_1 - \varphi_2)] \rangle \rangle \langle \langle \cos[n(\varphi_1 - \varphi_2)] \rangle \rangle \\ &= \langle v_m^2 v_n^2 \rangle - \langle v_m^2 \rangle \langle v_n^2 \rangle. \end{aligned} \quad (4)$$

The subscript c indicates the cumulant. Positive (Negative) values of $SC(m, n)$ suggest the correlation (anti-correlation) between v_m^2 and v_n^2 , which means that if v_m^2 is larger than $\langle v_m^2 \rangle$ in an event then the probability of v_n^2 being larger than $\langle v_n^2 \rangle$ in that same event is enhanced (suppressed). The $SC(m, n)$ observables focus on the correlations among different orders of flow harmonics and enable the quantitative comparison between experimental data and model calculations. To eliminate the effect of the magnitudes of v_m and v_n on the value of the symmetric cumulant, we divide $SC(m, n)$ by their average values, $\langle v_m^2 \rangle$ and $\langle v_n^2 \rangle$, and define the normalized symmetric cumulant. This enables us to compare data and model calculations in a quantitative way and compare the fluctuations of the initial and final states. The normalized symmetric cumulant, denoted by $NSC(m, n)$, is achieved following the standard method from Ref. [37]:

$$NSC(m, n) = \frac{SC(m, n)}{\langle v_m^2 \rangle \langle v_n^2 \rangle}. \quad (5)$$

These correlations have been measured by both STAR experiment at RHIC [38] and ALICE experiment at LHC [39] with the observation of a positive correlation between v_2 and v_4 while a negative correlation between v_2 and v_3 . The sensitivity of these observables to the shear viscosity to entropy density (η/s) has been studied in transport models like AMPT [40].

B. Asymmetric Cumulants of Flow Amplitudes

Recent studies indicate that insightful information can be obtained about the properties of Quark-Gluon Plasma

by using higher-order observables [41]. These observables can probe the genuine correlations between the different moments of different flow harmonics. They are robust against non-flow correlations, which can be verified using the HIJING Monte Carlo generator [42]. The asymmetric cumulant $AC_{2,1}(m, n)$ is defined as [35]

$$\begin{aligned} AC_{2,1}(m, n) &\equiv \langle \langle v_m^2 v_n^2 \rangle \rangle_c \equiv \langle v_m^4 v_n^2 \rangle_c \\ &= \langle v_m^4 v_n^2 \rangle - \langle v_m^4 \rangle \langle v_n^2 \rangle - 2 \langle v_m^2 v_n^2 \rangle \langle v_m^2 \rangle \\ &\quad + 2 \langle v_m^2 \rangle^2 \langle v_n^2 \rangle \end{aligned} \quad (6)$$

In Eq. (6), the subscript (2,1) on the left-hand side indicates the exponents of v_m^2 and v_n^2 on the right-hand side. The combinations of azimuthal correlators used to estimate the *ACs* are [35]:

$$\begin{aligned} AC_{2,1}(m, n) &= \langle \langle e^{i(m\varphi_1 + m\varphi_2 + n\varphi_3 - m\varphi_4 - m\varphi_5 - n\varphi_6)} \rangle \rangle \\ &\quad - \langle \langle e^{i(m\varphi_1 + m\varphi_2 - m\varphi_3 - m\varphi_4)} \rangle \rangle \langle \langle e^{i(n\varphi_1 - n\varphi_2)} \rangle \rangle \\ &\quad - 2 \langle \langle e^{i(m\varphi_1 + n\varphi_2 - m\varphi_3 - n\varphi_4)} \rangle \rangle \langle \langle e^{i(m\varphi_1 - m\varphi_2)} \rangle \rangle \\ &\quad + 2 \langle \langle e^{i(m\varphi_1 - m\varphi_2)} \rangle \rangle^2 \langle \langle e^{i(n\varphi_1 - n\varphi_2)} \rangle \rangle \end{aligned} \quad (7)$$

These expressions are genuine multivariate cumulants. $AC_{1,1}(m, n)$ corresponds to $SC(m, n)$, illustrating the generalisation aspect of the *ACs*. We can also normalize the *ACs*. This procedure has two benefits. Normalizing the results allows proper comparisons and determination of the initial state effects and the changes brought by the hydrodynamic evolution since the predictions for *ACs* in the initial and final state do not have the same scale. Flow amplitudes depend on the transverse momentum, p_T , which leads to a similar dependence in any linear combinations of them, such as the *SCs* and the *ACs*. The normalization eliminates this dependence and enables comparisons between models and data with different p_T ranges [42]. Again, the normalization of the *ACs* is done following the standard method from Ref. [37],

$$NAC_{2,1}(m, n) = \frac{AC_{2,1}(m, n)}{\langle v_m^2 \rangle^2 \langle v_n^2 \rangle}. \quad (8)$$

In this paper, we have presented the measurement of $SC(m, n)$ and $AC_{2,1}(m, n)$ in Au+Au collisions at $\sqrt{s_{NN}} = 200$ GeV using a hybrid hydrodynamic model. $SC(m, n)$ have been computed in previous studies from hydrodynamic and transport models [37, 42–48], while $AC_{2,1}(m, n)$ have been computed in transport models [46, 47]. ALICE collaboration has performed a systemic study of $SC(m, n)$ and $NSC(m, n)$ [49]. ALICE collaboration has also measured $AC_{2,1}(m, n)$ for Pb+Pb collisions at $\sqrt{s_{NN}} = 5.02$ TeV [50]. In addition to symmetric cumulants, various other correlators have also been studied [51–54]. We show the sensitivity of these measurements to the transport properties, such as the shear viscosity to entropy density ratio, η/s , and the bulk viscosity to entropy density ratio, ζ/s , of the medium.

II. FRAMEWORK

We use a framework with multiple components to simulate various stages of heavy ion collisions. The hydrodynamic evolution has been initialized using a Glauber-based model. To generate the incoming nuclei, we use a Woods-Saxon distribution to sample nucleons.

$$\rho = \frac{\rho_0}{1 + \exp[(r - R)/a]}. \quad (9)$$

Here, $r = \sqrt{x^2 + y^2 + z^2}$, a characterizes the diffuseness of the nuclear surface, R is the radius parameter, and ρ_0 is the saturation density determined by $\int \rho dr^3 = A$ (mass number of the nucleus). We have taken $R = 6.38$ fm, and $a = 0.535$ fm [55].

The evolution of the energy-momentum tensor starts at $\tau_0 = 0.6$ fm. The hydrodynamic equations are solved using the Music simulation [56–59], which utilizes a Kurganov-Tadmor algorithm. A constant effective $\eta/s = 0.08$ was fixed by reproducing the measured anisotropic flow coefficients of charged hadrons. We use a temperature-dependent specific bulk viscosity parametrized in the following way [60]:

$$\frac{\zeta}{s} = \begin{cases} \lambda_1 e^{-(x-1)/\sigma_1} + \lambda_2 e^{-(x-1)/\sigma_2} + 0.001 & (T > 1.05T_C) \\ \lambda_3 e^{(x-1)/\sigma_3} + \lambda_4 e^{(x-1)/\sigma_4} + 0.03 & (T < 0.995T_C) \end{cases}$$

where $x = T/T_C$. The fitted parameters are $\lambda_1 = \lambda_3 = 0.9$, $\lambda_2 = 0.25$, $\lambda_4 = 0.22$, $\sigma_1 = 0.025$, $\sigma_2 = 0.13$, $\sigma_3 = 0.0025$, $\sigma_4 = 0.022$, $A_1 = -13.77$, $A_2 = 27.55$ and $A_3 = 13.45$.

We use a QCD equation of state (EoS), N EOS-B [61], based on continuum extrapolated lattice calculations at zero net baryon chemical potential published by the HotQCD Collaboration [62–64]. It is smoothly matched to a hadron resonance gas EoS in the temperature region between 110 and 130 MeV [65].

A hyper-surface is generated from the hydrodynamic space-time evolution of the fluid. To describe the dilute hadronic phase, we utilize the iSS code [66, 67] to sample the primordial hadrons from the hypersurface with a constant energy density, $e_{sw} = 0.26 \text{ GeV}/fm^3$, equivalent to a local temperature of approximately 151 MeV. Then, we use the UrQMD code [68, 69] to simulate scatterings and decays of hadrons during the late stage of heavy ion collisions. To increase statistics, each hydrodynamic switching hyper-surface is sampled multiple times. The number of oversampling events for every hydrodynamic event is determined to ensure sufficient statistics for every centrality class. We generated ensembles of 2000 hydrodynamic events for each centrality class, each with a suitable number of repeated samplings. Table I lists the number of events generated for each of the centrality classes with the three sets of parameters for the hydrodynamic stage shown in Table II. Table III outlines the particles used in the analyses at the end of different stages of the evolution. Analysis at the end of:

Centrality class	0-10%	10-20%	20-30%	30-40%	40-50%
# Events ($\times 10^6$)	4	6	8	3	4

TABLE I. Ensemble size (in millions) of the centrality classes at the end of Stage III.

	η/s	ζ/s
Parameter(Par.) Set I	0	0
Parameter(Par.) Set II	0.08	0
Parameter(Par.) Set III	0.08	$\zeta/s(T)$

TABLE II. The transport coefficients' values for the parameter sets used in the ensembles generated for this study.

	Particle list
Stage I	Hydrodynamic evolution + particlization (Primordial)
Stage II	Primordial + Resonance decays
Stage III	Primordial + UrQMD

TABLE III. The particle lists analyzed at the end of different stages of the evolution (Hydrodynamic evolution, resonance decay, and hadronic transport).

Centrality class	$\langle N_{part} \rangle$
0-10%	327.7
10-20%	240.3
20-30%	172.7
30-40%	120.5
40-50%	81.5

TABLE IV. $\langle N_{part} \rangle$ in the centrality classes from a Monte-Carlo Glauber model.

- stage I includes hydrodynamic evolution and particlization,
- stage II includes hydrodynamic evolution, particlization, and resonance decay, and
- stage III includes hydrodynamic evolution, particlization, resonance decay, and hadronic interactions within the UrQMD model approach.

In the following results, some observables will be presented by scaling with the average number of participants, $\langle N_{part} \rangle$. Table IV lists the values of $\langle N_{part} \rangle$ in different centrality bins, which are determined using the Monte-Carlo Glauber model. The $SC(m, n)$ and $AC_{2,1}(m, n)$ observables have been computed using particles with transverse momentum (p_T) ranges of $[0.2, 2.0]$ GeV and $[0.01, 3.0]$ GeV, respectively.

III. ERROR ESTIMATION

The bootstrap method is used to efficiently estimate the error on ensemble-level observables using the Monte-Carlo approach, bypassing the complexities of standard error propagation. It involves randomly selecting events with replacement from an original sample to create bootstrap samples, allowing for the calculation of sampling variance.

Let \hat{O} be the estimator of a statistic on which we intend to find the standard error. To estimate the standard error using the bootstrap method, follow these steps:

- Given a parent sample of size n , construct B independent bootstrap samples $X_1^*, X_2^*, \dots, X_B^*$, each with n data points randomly drawn with replacement.
- Evaluate the estimator for each bootstrap sample.

$$\hat{O}_b^* = \hat{O}(X_b^*), \quad b = 1, 2, \dots, B.$$

- The sampling variance of the estimator can then be calculated as follows:

$$Var(\hat{O}) = \frac{1}{B-1} \sum_{b=1}^B (\hat{O}_b^* - \bar{\hat{O}})^2,$$

$$\text{where, } \bar{\hat{O}} = \frac{1}{B} \sum_{b=1}^B \hat{O}_b^*.$$

The optimal value of B for accurate error estimation varies, but generally, larger values yield better estimates.

IV. RESULTS

We calibrated our model by using the produced particle yields, transverse momentum spectra and elliptic flow. We then compared these results to experimental data from the PHENIX and STAR Collaborations. The normalization factor for the system's energy density was determined by matching the model and STAR data [70] charged hadron multiplicity $dN_{Ch}/d\eta$ in the 0-5% centrality bin. We also compared the p_T spectra of identified particles in 0-5% centrality Au+Au collisions to STAR results [70]. Additionally, we compared the single-particle anisotropic flow coefficient v_2 of charged particles in 20-30% centrality Au+Au collisions with the PHENIX measurement [71]. The hydrodynamic evolution of the MCGM initial conditions, coupled to UrQMD, can reproduce the elliptic flow up to the mid-central collisions.

A. Sensitivity to transport coefficients

1. Four-particle symmetric cumulants

In this section, we present the results for $SC(m, n)$ and $NSC(m, n)$ obtained from our simulations. To evaluate their sensitivity to the hydro transport coefficients, we computed these observables using the three sets of ensembles listed in Table II.

We found that both $SC(2, 3)$ and $SC(2, 4)$ are suppressed by the effects of shear and bulk viscosities. In Fig.[1], we illustrate how shear viscosity influences $v_2\{4\}$ and $SC(2, 3)$. For $v_2\{4\}$, the maximum change observed is about 10% in mid-central collisions. In contrast,

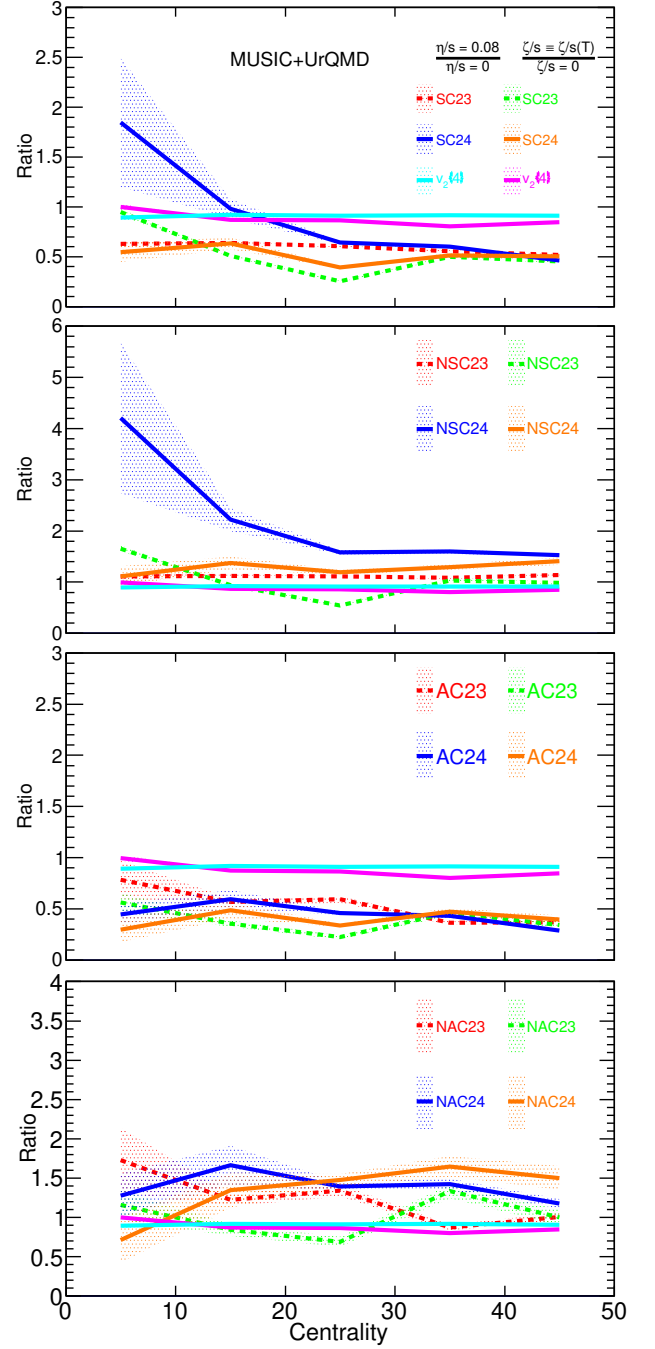


FIG. 1. Ratios of $v_2\{4\}$, $SC(2, n)$, $NSC(2, n)$, $AC_{2,1}(2, n)$, and $NAC_{2,1}(2, n)$, with different hydro parameter sets, vs centrality in Au+Au collisions at $\sqrt{s_{NN}} = 200$ GeV. The figure compares the effects of η/s and ζ/s on $v_2\{4\}$, $SC(2, n)$, $NSC(2, n)$, $AC_{2,1}(2, n)$, and $NAC_{2,1}(2, n)$. The plotted results show ratios of $v_2\{4\}$ using cyan (η/s) and magenta (ζ/s) bands and $SC(2, n)$, $NSC(2, n)$, $AC_{2,1}(2, n)$, and $NAC_{2,1}(2, n)$ using red ($n=3$, η/s), green ($n=3$, ζ/s), blue ($n=4$, η/s) and orange ($n=4$, ζ/s) bands. In the legends, the left column show the ratios for checking the effect of η/s and the right column show the ratios for checking the effect of ζ/s .

SC(2, 3) shows a change of approximately 40-50% across the centrality range. We also noted a similar dependence on the bulk viscosity of the medium, indicating that these observables are particularly sensitive to the transport coefficients.

The transport coefficients have more significant effects on SC(2, 4) than on SC(2, 3). A comparison of symmetric cumulants with $v_3\{4\}$ reveals a similar difference in their sensitivity to shear and bulk viscosities. It should be noted that $v_n\{4\}$ is more sensitive to the transport coefficients as n increases [72]. This large sensitivity of symmetric cumulants primarily arises from the characteristics of anisotropic flow, as the symmetric cumulants involve higher powers of flow coefficients.

As discussed in the introduction, normalization removes the effect of the magnitudes of v_m and v_n on the value of the symmetric cumulant. Therefore, it should also eliminate the incidental sensitivity of SC(m, n) to shear and bulk viscosity. So, we also examined the sensitivities of the normalized cumulants. From Fig.[1], we observe that NSC(2, 3) shows little sensitivity to shear viscosity. However, NSC(2, 4) is more sensitive to both shear and bulk viscosities than $v_2\{4\}$.

2. Six-particle asymmetric cumulants

Now, we present the results for $AC_{2,1}(m, n)$. In Fig. 1, we illustrate the effect of shear viscosity on $v_2\{4\}$ and $AC_{2,1}(m, n)$. For $AC_{2,1}(2, 4)$, we observe a change of approximately 50% across the centrality range, although it is important to note that the 0-10% and 10-20% centrality classes contain large statistical uncertainties. We also find that the medium's bulk viscosity similarly influences these observables.

The effects of the transport coefficients is found to be greater on $AC_{2,1}(2, 4)$ than on $AC_{2,1}(2, 3)$. Compared to traditional flow observables, these observables are more sensitive to transport coefficients. This magnified of asymmetric cumulants sensitivity primarily stems from the characteristics of anisotropic flow, as the asymmetric cumulants involve higher powers of flow.

As discussed in the introduction, normalization removes the effect of the magnitudes of v_m and v_n on the value of the asymmetric cumulant. Therefore, it should also eliminate the incidental sensitivity of $AC_{2,1}(m, n)$ to shear and bulk viscosity. So, we also examined the sensitivities of the normalized asymmetric cumulants. From Fig.[1], it is evident that $NAC_{2,1}(2, 3)$ shows little sensitivity to shear viscosity. In contrast, $NAC_{2,1}(2, 4)$ demonstrates greater sensitivity to both shear and bulk viscosities compared to $v_2\{4\}$.

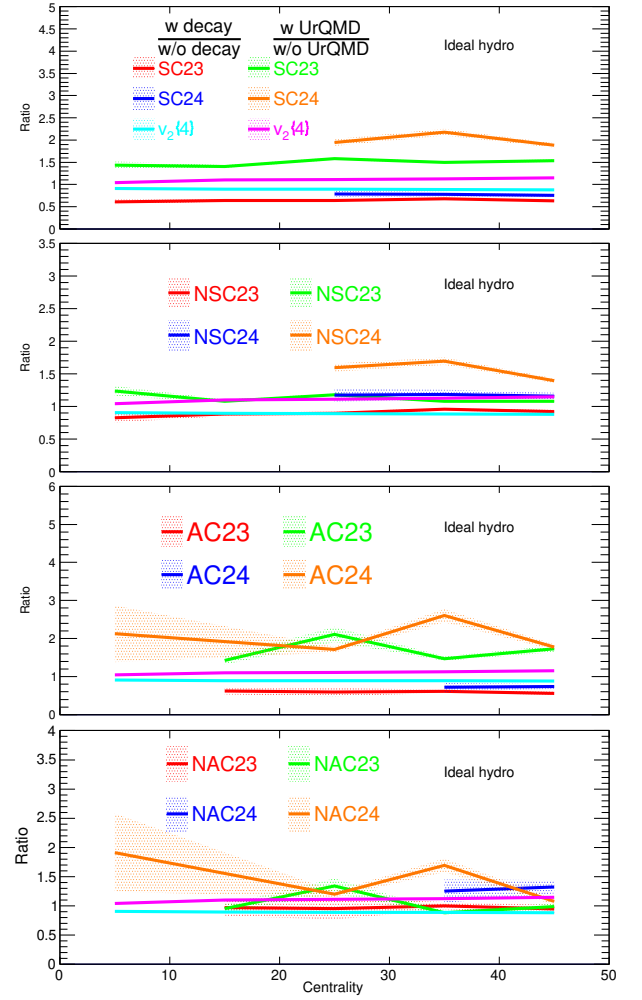


FIG. 2. Ratios of $v_2\{4\}$, SC(2, n), NSC(2, n), $AC_{2,1}(2, n)$, and $NAC_{2,1}(2, n)$, computed at the three different stages of the evolution, vs centrality in Au+Au collisions at $\sqrt{s_{NN}} = 200$ GeV. The figure compares the effects of resonance decay and hadronic interactions on $v_2\{4\}$, SC(2, n), NSC(2, n), $AC_{2,1}(2, n)$, and $NAC_{2,1}(2, n)$. The plotted results show ratios of $v_2\{4\}$ using cyan (resonance decay) and magenta (hadronic interactions) bands and SC(2, n), NSC(2, n), $AC_{2,1}(2, n)$, and $NAC_{2,1}(2, n)$ using red ($n=3$, resonance decay), green ($n=3$, hadronic interactions), blue ($n=4$, resonance decay) and orange ($n=4$, hadronic interactions) bands. In the legends, the left column show the ratios for checking the effect of resonance decay and the right column show the ratios for checking the effect of hadronic interactions.

B. Sensitivity to hadronic interactions

1. Four-particle symmetric cumulants

The hadronic afterburner plays a crucial role in interpreting data collected at RHIC [44]. To assess the sensitivity to hadronic interactions and resonance decay, we computed various observables at the end of the three stages of evolution mentioned in Table III. We found that

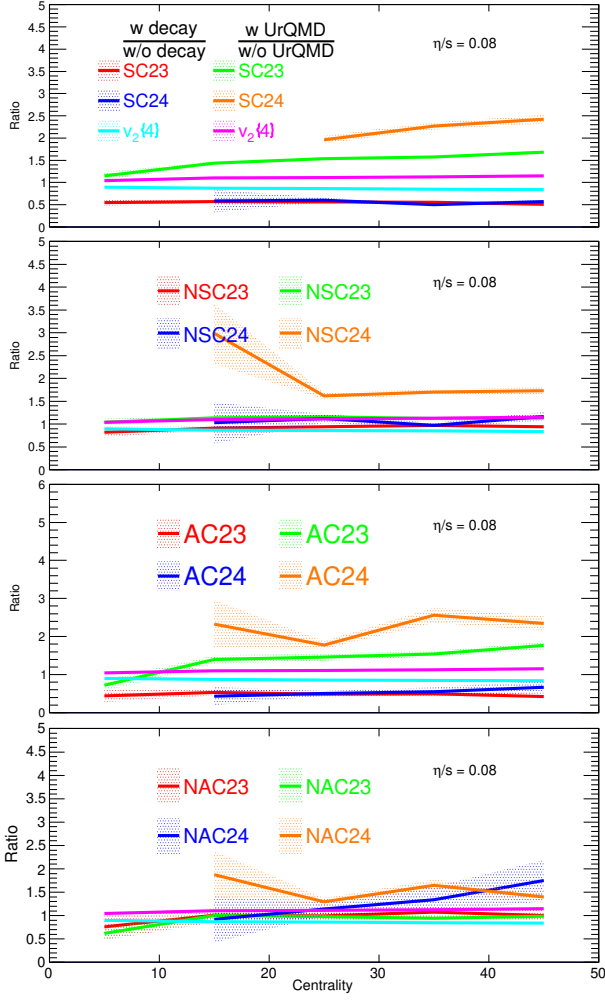


FIG. 3. Ratios of $v_2\{4\}$, $SC(2,n)$, $NSC(2,n)$, $AC_{2,1}(2,n)$, and $NAC_{2,1}(2,n)$, computed at the three different stages of the evolution, vs centrality in Au+Au collisions at $\sqrt{s_{NN}} = 200$ GeV. The figure compares the effects of resonance decay and hadronic interactions on $v_2\{4\}$, $SC(2,n)$, $NSC(2,n)$, $AC_{2,1}(2,n)$, and $NAC_{2,1}(2,n)$. The plotted results show ratios of $v_2\{4\}$ using cyan (resonance decay) and magenta (hadronic interactions) bands and $SC(2,n)$, $NSC(2,n)$, $AC_{2,1}(2,n)$, and $NAC_{2,1}(2,n)$ using red ($n=3$, resonance decay), green ($n=3$, hadronic interactions), blue ($n=4$, resonance decay) and orange ($n=4$, hadronic interactions) bands. In the legends, the left column show the ratios for checking the effect of resonance decay and the right column show the ratios for checking the effect of hadronic interactions.

both $SC(2,3)$ and $SC(2,4)$ are suppressed by resonance decay and enhanced by hadronic interactions; however, the magnitudes of these effects differ between the two observables.

In Figs. [2][3][4], we illustrate how resonance decay and hadronic interactions impact $v_2\{4\}$ and $SC(2,3)$. For $v_2\{4\}$, we observe a change of about 15% due to resonance decay, with an additional 5% change due to both hadronic interactions and resonance decay in mid-central

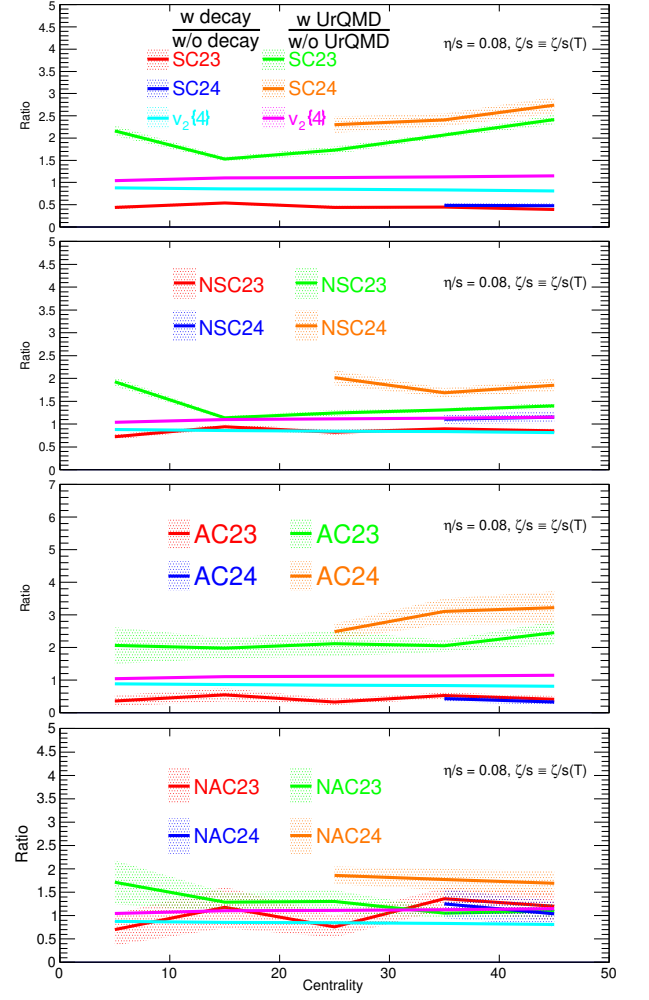


FIG. 4. Ratios of $v_2\{4\}$, $SC(2,n)$, $NSC(2,n)$, $AC_{2,1}(2,n)$, and $NAC_{2,1}(2,n)$, computed at the three different stages of the evolution, vs centrality in Au+Au collisions at $\sqrt{s_{NN}} = 200$ GeV. The figure compares the effects of resonance decay and hadronic interactions on $v_2\{4\}$, $SC(2,n)$, $NSC(2,n)$, $AC_{2,1}(2,n)$, and $NAC_{2,1}(2,n)$. The plotted results show ratios of $v_2\{4\}$ using cyan (resonance decay) and magenta (hadronic interactions) bands and $SC(2,n)$, $NSC(2,n)$, $AC_{2,1}(2,n)$, and $NAC_{2,1}(2,n)$ using red ($n=3$, resonance decay), green ($n=3$, hadronic interactions), blue ($n=4$, resonance decay) and orange ($n=4$, hadronic interactions) bands. In the legends, the left column show the ratios for checking the effect of resonance decay and the right column show the ratios for checking the effect of hadronic interactions.

collisions. In contrast, $SC(2,3)$ shows a change of approximately 40% due to resonance decay across the entire centrality range and a change of 40-60% due to the combined effects of hadronic interactions and resonance decay. $SC(2,4)$ is affected more strongly by resonance decay and late-stage hadronic interactions than $SC(2,3)$. These observables, therefore, demonstrate higher sensitivity to resonance decay and hadronic interactions. The comparison of the symmetric cumulants with $v_3\{4\}$ also

indicates similar differences in sensitivity to these effects. This increased sensitivity of symmetric cumulants arises mainly from anisotropic flow, with symmetric cumulants incorporating higher powers of flow.

As discussed in the introduction, normalization removes the effect of the magnitudes of v_m and v_n on the value of the symmetric cumulant. Therefore, it should also eliminate the incidental sensitivity of $SC(m, n)$ to resonance decay and late-stage hadronic interactions. So, we also examined the sensitivities of the normalized symmetric cumulants. From Figs. [2][3][4], it is clear that $NSC(2, 3)$ shows little sensitivity to either resonance decay or late-stage hadronic interactions (UrQMD). In contrast, $NSC(2, 4)$ exhibits greater sensitivity to both resonance decay and late-stage hadronic interactions compared to $v_2\{4\}$.

2. Six-particle asymmetric cumulants

Now, we present the results for $AC_{2,1}(m, n)$. In Figs.[2][3][4], we show the effects of resonance decay and hadronic interactions on elliptic flow from the four-particle correlations and $AC_{2,1}(2, 3)$. For $AC_{2,1}(2, 3)$, we see a change of around 40% due to these in the mid-central collisions. The effects of resonance decay and late-stage hadronic interactions are found to be greater on $AC_{2,1}(2, 4)$ than on $AC_{2,1}(2, 3)$. Compared to the traditional flow observables, we see that these are more sensitive to resonance decay and hadronic interactions. This magnified sensitivity of asymmetric cumulants can be attributed to the properties of anisotropic flow, particularly as the asymmetric cumulants incorporate higher powers of flow.

As discussed in the introduction, normalization removes the effect of the magnitudes of v_m and v_n on the value of the symmetric cumulant. Therefore, it should also eliminate the incidental sensitivity of $SC(m, n)$ to resonance decay and late-stage hadronic interactions. So, we also investigated the sensitivities of the normalized asymmetric cumulants. From Figures [2][3][4], it is evident that $NAC_{2,1}(2, 3)$ shows minimal sensitivity to both resonance decay and late-stage hadronic interactions (as represented by the UrQMD model). In contrast, $NAC_{2,1}(2, 4)$ demonstrates significantly greater sensitivity to these factors compared to $v_2\{4\}$. Therefore, these normalized cumulant measurements have the potential to differentiate between various transport models. Additionally, we examined the sensitivities of the normalized cumulants. From Figs. [2][3][4], it is clear that $NAC_{2,1}(2, 3)$ shows little sensitivity to either resonance decay or late-stage hadronic interactions (UrQMD). In contrast, $NAC_{2,1}(2, 4)$ exhibits greater sensitivity to both resonance decay and late-stage hadronic interactions compared to $v_2\{4\}$.

As a result, these normalized (a)symmetric cumulant measurements have the potential to differentiate between

various models of quark-gluon plasma (QGP) evolution in hydrodynamic and transport models. $NSC(2, 3)$ and $NAC_{2,1}(2, 3)$, due to their insensitivity to hydro model parameters, resonance decay, and late-stage hadronic interactions, are particularly useful for constraining the initial state of the system's evolution.

C. Centrality dependence of $SC(m, n)$ and $AC_{2,1}(m, n)$

1. Four-particle symmetric cumulants

Next, we compare the results from our simulations with the experimental measurements from RHIC. $SC(m, n)$ have been computed in previous studies from hydrodynamic and transport models [37, 42, 44–48], while $AC_{2,1}(m, n)$ have been computed in some transport models [46, 47]. Fig. [5] shows comparisons between the theory calculations for the symmetric cumulants $SC(2, 3)$ and $SC(2, 4)$ multiplied by $\langle N_{part} \rangle$ and the same measured by the STAR Collaboration [73]. The factor of $\langle N_{part} \rangle$ is multiplied to scale out the trivial dilution of correlation with the increase in the number of multiplets. We are able to reproduce the qualitative variations with centrality. The magnitudes of $\langle N_{part} \rangle SC(2, 3)$ and $\langle N_{part} \rangle SC(2, 4)$ increase from central to mid-peripheral events and then again decreases for very peripheral events. Here, we do not aim to reproduce the experimental data because our aim is to check the sensitivity of these observables to the transport properties of the system created in these collisions. The comparison in Fig.[5] reflects that the correlation in initial spatial eccentricities and the following hydrodynamic evolution can capture the correlation among flow harmonics of different orders. Negative values of $SC(2, 3)$ throughout the centrality range reveal the anti-correlation between v_2 and v_3 . While as $SC(2, 4)$ is positive for all centralities, indicating positive correlations between v_2 and v_4 . Symmetric cumulants do not have contributions from non-flow effects, where non-flow refers to azimuthal correlations not related to the reaction plane orientation, like those from resonances, jets, quantum statistics, etc. This is verified by computing these observables for the HIJING model, which includes only non-flow physics, for which these are consistently zero [35]. The model captures the variation of $SC(m, n)$ with the centrality. In central collisions, the model underestimates $SC(2, 4)$, possibly due to inadequate fluctuations in the initial conditions or some shortcomings in the transport model since the nonlinear response in v_4 and ε_4 is sensitive to these effects. However, $SC(2, 3)$ is better aligned with the data because the $v_2 - v_3$ correlations mainly arise from the initial state $\varepsilon_2 - \varepsilon_3$ correlations due to linear response in v_2 and v_3 .

The normalized symmetric cumulants in Au+Au collisions at $\sqrt{s_{NN}} = 200$ GeV, computed using Eq.[5] in momentum space and the corresponding equation in coordinate space for the initial state eccentricity (Eq.[10])

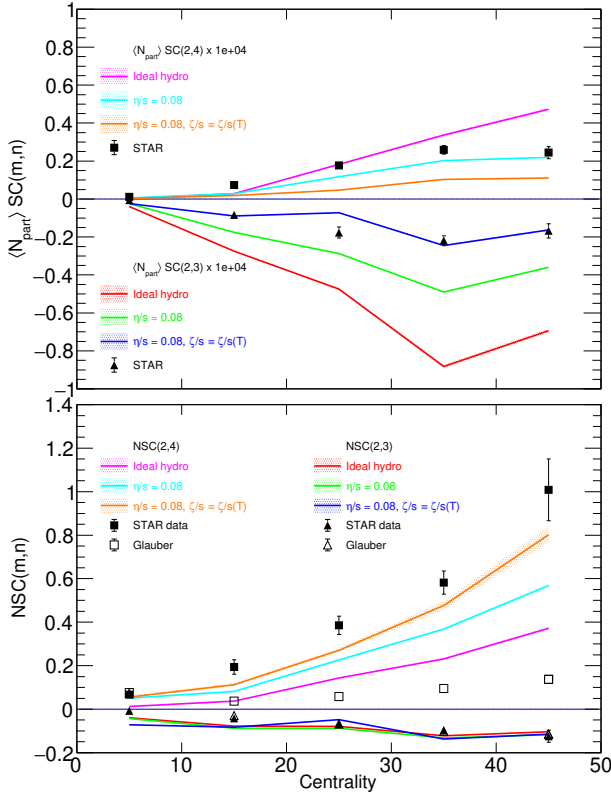


FIG. 5. (Normalized) Symmetric cumulant vs centrality from four-particle correlations compared with STAR data [73] in Au+Au collisions at $\sqrt{s_{NN}} = 200$ GeV. $SC(2,3)$ is consistently negative while as $SC(2,4)$ is consistently positive.

evaluated using the Monte Carlo Glauber model, are presented in Fig.[5]. We observe that $NSC(2,3)$ shows little sensitivity to shear and bulk viscosities. However, $NSC(2,4)$ is more sensitive to both shear and bulk viscosities than $v_2\{4\}$. This is due to the fact that v_4 is the superposition of a nonlinear term that is proportional to $(v_2)^2$ and a linear term v_{4L} . This can be expressed as:

$$v_4 = v_{4L} + \chi_4(v_2)^2,$$

where χ_4 is the non-linear response coefficient. The term v_{4L} is damped more strongly than the nonlinear term, as noted in Reference [74]. Additionally, v_{4L} is less correlated with v_2 . Consequently, as viscosity increases, the correlation between v_4 and v_2 also increases.

$$\varepsilon_n e^{in\psi_n} = -\frac{\int r^n e^{in\phi} \rho(r, \phi) r dr d\phi}{\int r^n \rho(r, \phi) r dr d\phi}, n \geq 2 \quad (10)$$

If only eccentricity drives v_n , then we can expect that the $NSC(m,n)$ in the final state would be equal to the $NSC(m,n)$ in the initial state. Fig.[5] shows that the initial anti-correlation between ε_2 and ε_3 is mainly responsible for the observed anti-correlation between v_2 and v_3 . However, the correlation between ε_2 and ε_4 is smaller than the observed correlation between v_2 and v_4 . The contribution to anisotropic flow v_4 not only comes

from the linear response of the system to ε_4 but also has a contribution proportional to ε_2^2 . As collisions become more peripheral, the difference between $NSC(2,4)$ in the final state and the initial state increases, likely due to ε_2 playing a more significant role in v_4 . This has also been observed in Pb+Pb collisions at $\sqrt{s_{NN}} = 2.76$ TeV by the ATLAS [75] and ALICE [39] experiments. The properties of the medium were suggested to affect the relative contribution of ε_2 in v_4 compared to ε_4 [74]. Therefore, $NSC(2,4)$ provides a probe into the medium properties.

2. Six-particle asymmetric cumulants

$AC_{2,1}(m,n)$ have measured by the ALICE collaboration for Pb+Pb collisions at $\sqrt{s_{NN}} = 5.02$ TeV [50]. In Fig.[6], we show the centrality dependence of $AC_{2,1}(m,n)$, multiplied by $\langle N_{part} \rangle$ to scale out the trivial dilution of correlation with the increase in the number of multiplets, for Au+Au at $\sqrt{s_{NN}} = 200$ GeV. The magnitudes of $\langle N_{part} \rangle AC_{2,1}(2,3)$ and $\langle N_{part} \rangle AC_{2,1}(2,4)$ increase with centrality. The trends are similar to the results by the ALICE collaboration. As for symmetric cumulants, negative values of $AC(2,3)$ throughout the centrality range reveal the anti-correlation between v_2 and v_3 . While as $AC(2,4)$ is positive for all centralities, indicating positive correlations between v_2 and v_4 . We compute these observables for the three sets of ensembles mentioned in Table II and observe that both $AC_{2,1}(2,3)$ and $AC_{2,1}(2,4)$ are suppressed by shear and bulk viscosities. As discussed earlier, the linear component in v_4 is damped more significantly than the nonlinear term and shows a weaker correlation with v_2 . Thus, as viscosity increases, the correlation between v_4 and v_2 is also enhanced.

In Fig.[6], we have compared the normalized asymmetric cumulant in coordinate and momentum space, as computed using Eq.[8] and the corresponding equation for the initial state eccentricities (Eq.[10]). Again, if only eccentricity drives v_n , we can expect the $NAC_{2,1}(m,n)$ in the final state to be equal to the $NAC_{2,1}(m,n)$ in the initial state. Fig. [6] illustrates that the initial negative correlation between ε_2 and ε_3 primarily causes the observed negative correlation between v_2 and v_3 . However, unlike symmetric cumulants, here, the initial state correlations are smaller in the peripheral collisions. The correlation between ε_2 and ε_4 is weaker than the correlation observed between v_2 and v_4 . The contribution to anisotropic flow v_4 comes not only from the linear response of the system to ε_4 , but also from a contribution proportional to ε_2^2 . As collisions become more peripheral, the difference between $NAC(2,4)$ in the final state and the initial state increases. This is likely due to ε_2 playing a more significant role in v_4 .

Currently, STAR has not yet measured asymmetric cumulants. We conducted a comparison between our findings and the Pb+Pb 5.02 TeV results from ALICE (See Appendix Fig.[7] and Fig.[8]). The centrality dependence

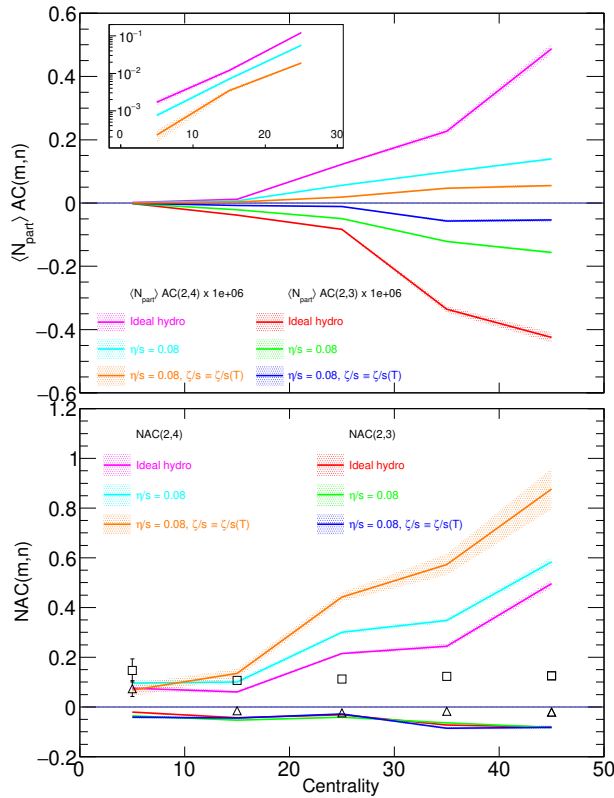


FIG. 6. (Normalized) Asymmetric cumulant vs centrality from six-particle correlations in Au+Au collisions at $\sqrt{s_{NN}} = 200$ GeV. $AC_{2,1}(2,3)$ is consistently negative while as $AC_{2,1}(2,4)$ is consistently positive.

of the observables we discussed in this paper shows similarities between ALICE and STAR data. The $SC(m,n)$ values are about an order of magnitude larger at ALICE than at STAR. Similarly, the $AC_{21}(m,n)$ values are 3 to 5 times larger at ALICE compared to STAR. However, the similarities in the magnitude and centrality dependence of the normalized cumulants are noteworthy. This comparison indicates minimal energy dependence for the normalized cumulants.

D. Conclusions

We have presented results for multi-particle correlation functions in heavy-ion collisions at top RHIC energy using a hybrid framework based on the Monte-Carlo Glauber model, MUSIC viscous hydrodynamics simulations, and the UrQMD hadronic cascade.

First, we adjusted the free parameters, such as shear

and bulk viscosities, to describe particle multiplicities, mean transverse momentum, and anisotropic flow. After that, we discussed the impact of shear and bulk viscosities, resonance decay, and hadronic interactions on traditional and novel observables.

We have studied correlators that measure the correlations between flow harmonics of varying orders, specifically four and six-particle correlations, including both symmetric and asymmetric cumulants as functions of centrality at midrapidity in Au+Au collisions at $\sqrt{s_{NN}} = 200$ GeV. These observables are very sensitive to shear and bulk viscosities, resonance decay, and hadronic interactions. However, this magnified sensitivity can be attributed to the properties of anisotropic flow, particularly as the cumulants incorporate higher powers of flow. We then checked the sensitivities of the normalized cumulants. We found that $NSC(2,3)$ and $NAC_{2,1}(2,3)$ are insensitive to both the hydro model parameters (shear and bulk viscosity) and late-stage hadronic interactions. This strongly supports their effectiveness as reliable tools for constraining the initial state of the system's evolution. Conversely, $NSC(2,4)$ and $NAC_{2,1}(2,4)$ show considerable sensitivity to these stages, allowing them to effectively constrain hydrodynamic and transport models.

A single parameter set of transport coefficients is unable to explain $SC(2,3)$ and $SC(2,4)$ simultaneously.

We observed anti-correlation between event-by-event fluctuations of v_2 and v_3 , while the event-by-event fluctuations of v_2 and v_4 are found to be positively correlated. The observed anti-correlation between v_2 and v_3 appears to be described by the initial-stage anti-correlation between ε_2 and ε_3 , which supports the idea of linearity between ε_n and v_n [23]. The hydrodynamic response suggests that the final state fluctuation originates from the initial state. However, including the nonlinear hydrodynamic response of the medium is necessary to reproduce the measured correlation between v_2 and v_4 , as the initial-stage linear correlation alone is insufficient.

The values of $SC(m,n)$ and $AC_{21}(m,n)$ at ALICE are larger—by factors ranging from 3 to 8—compared to those at STAR. However, it is important to note the similarities in the magnitude and centrality dependence of the normalized cumulants. This comparison indicates that there is minimal energy dependence for the normalized cumulants.

E. Acknowledgements

We would like to acknowledge Tribhuban Parida for fruitful discussions and providing us the computational setup.

[1] J. C. Collins and M. J. Perry, Superdense Matter: Neutrons Or Asymptotically Free Quarks?,

Phys. Rev. Lett. **34**, 1353 (1975).

- [2] E. V. Shuryak, What RHIC experiments and theory tell us about properties of quark-gluon plasma?, *Nucl. Phys. A* **750**, 64 (2005), arXiv:hep-ph/0405066.
- [3] W. Busza, K. Rajagopal, and W. van der Schee, Heavy Ion Collisions: The Big Picture, and the Big Questions, *Ann. Rev. Nucl. Part. Sci.* **68**, 339 (2018), arXiv:1802.04801 [hep-ph].
- [4] K. H. Ackermann *et al.* (STAR), Elliptic flow in Au + Au collisions at $(\sqrt{s_{NN}})^{1/2} = 130$ GeV, *Phys. Rev. Lett.* **86**, 402 (2001), arXiv:nucl-ex/0009011.
- [5] B. I. Abelev *et al.* (STAR), Partonic flow and phi-meson production in Au + Au collisions at $\sqrt{s_{NN}} = 200$ -GeV, *Phys. Rev. Lett.* **99**, 112301 (2007), arXiv:nucl-ex/0703033.
- [6] K. Adcox *et al.* (PHENIX), Formation of dense partonic matter in relativistic nucleus-nucleus collisions at RHIC: Experimental evaluation by the PHENIX collaboration, *Nucl. Phys. A* **757**, 184 (2005), arXiv:nucl-ex/0410003.
- [7] U. Heinz and R. Snellings, Collective flow and viscosity in relativistic heavy-ion collisions, *Ann. Rev. Nucl. Part. Sci.* **63**, 123 (2013), arXiv:1301.2826 [nucl-th].
- [8] P. Braun-Munzinger, V. Koch, T. Schäfer, and J. Stachel, Properties of hot and dense matter from relativistic heavy ion collisions, *Phys. Rept.* **621**, 76 (2016), arXiv:1510.00442 [nucl-th].
- [9] S. Voloshin and Y. Zhang, Flow study in relativistic nuclear collisions by Fourier expansion of Azimuthal particle distributions, *Z. Phys. C* **70**, 665 (1996), arXiv:hep-ph/9407282.
- [10] J.-Y. Ollitrault, Anisotropy as a signature of transverse collective flow, *Phys. Rev. D* **46**, 229 (1992).
- [11] S. A. Bass, M. Gyulassy, H. Stoecker, and W. Greiner, Signatures of quark gluon plasma formation in high-energy heavy ion collisions: A Critical review, *J. Phys. G* **25**, R1 (1999), arXiv:hep-ph/9810281.
- [12] S. A. Voloshin, A. M. Poskanzer, and R. Snellings, Collective phenomena in non-central nuclear collisions, *Landolt-Bornstein* **23**, 293 (2010), arXiv:0809.2949 [nucl-ex].
- [13] S. A. Voloshin and A. M. Poskanzer, The Physics of the centrality dependence of elliptic flow, *Phys. Lett. B* **474**, 27 (2000), arXiv:nucl-th/9906075.
- [14] Y. B. Ivanov and A. A. Soldatov, Elliptic Flow in Heavy-Ion Collisions at Energies $\sqrt{s_{NN}} = 2.7$ -39 GeV, *Phys. Rev. C* **91**, 024914 (2015), arXiv:1401.2265 [nucl-th].
- [15] J. Adams *et al.* (STAR), Azimuthal anisotropy in Au+Au collisions at $\sqrt{s_{NN}} = 200$ -GeV, *Phys. Rev. C* **72**, 014904 (2005), arXiv:nucl-ex/0409033.
- [16] C. Adler *et al.* (STAR), Identified particle elliptic flow in Au + Au collisions at $\sqrt{s_{NN}} = 130$ -GeV, *Phys. Rev. Lett.* **87**, 182301 (2001), arXiv:nucl-ex/0107003.
- [17] K. Aamodt *et al.* (ALICE), Elliptic flow of charged particles in Pb-Pb collisions at 2.76 TeV, *Phys. Rev. Lett.* **105**, 252302 (2010), arXiv:1011.3914 [nucl-ex].
- [18] H. Sorge, Highly sensitive centrality dependence of elliptic flow: A novel signature of the phase transition in QCD, *Phys. Rev. Lett.* **82**, 2048 (1999), arXiv:nucl-th/9812057.
- [19] L. Adamczyk *et al.* (STAR), Third Harmonic Flow of Charged Particles in Au+Au Collisions at $\sqrt{s_{NN}} = 200$ GeV, *Phys. Rev. C* **88**, 014904 (2013), arXiv:1301.2187 [nucl-ex].
- [20] D. Solanki, P. Sorensen, S. Basu, R. Raniwala, and T. K. Nayak, Beam energy dependence of Elliptic and Triangular flow with the AMPT model, *Phys. Lett. B* **720**, 352 (2013), arXiv:1210.0512 [nucl-ex].
- [21] J. Adam *et al.* (ALICE), Higher harmonic flow coefficients of identified hadrons in Pb-Pb collisions at $\sqrt{s_{NN}} = 2.76$ TeV, *JHEP* **09**, 164, arXiv:1606.06057 [nucl-ex].
- [22] U. Heinz, Z. Qiu, and C. Shen, Fluctuating flow angles and anisotropic flow measurements, *Phys. Rev. C* **87**, 034913 (2013), arXiv:1302.3535 [nucl-th].
- [23] B. Alver and G. Roland, Collision geometry fluctuations and triangular flow in heavy-ion collisions, *Phys. Rev. C* **81**, 054905 (2010), [Erratum: *Phys. Rev. C* **82**, 039903 (2010)], arXiv:1003.0194 [nucl-th].
- [24] J. E. Parkkila, A. Onnerstad, and D. J. Kim, Bayesian estimation of the specific shear and bulk viscosity of the quark-gluon plasma with additional flow harmonic observables, *Phys. Rev. C* **104**, 054904 (2021), arXiv:2106.05019 [hep-ph].
- [25] E. Retinskaya, M. Luzum, and J.-Y. Ollitrault, Constraining models of initial state with v_2 and v_3 data from LHC and RHIC, *Nucl. Phys. A* **926**, 152 (2014), arXiv:1401.3241 [nucl-th].
- [26] C. Shen and U. Heinz, Collision Energy Dependence of Viscous Hydrodynamic Flow in Relativistic Heavy-Ion Collisions, *Phys. Rev. C* **85**, 054902 (2012), [Erratum: *Phys. Rev. C* **86**, 049903 (2012)], arXiv:1202.6620 [nucl-th].
- [27] D. Teaney, The Effects of viscosity on spectra, elliptic flow, and HBT radii, *Phys. Rev. C* **68**, 034913 (2003), arXiv:nucl-th/0301099.
- [28] C. Shen, S. A. Bass, T. Hirano, P. Huovinen, Z. Qiu, H. Song, and U. Heinz, The QGP shear viscosity: Elusive goal or just around the corner?, *J. Phys. G* **38**, 124045 (2011), arXiv:1106.6350 [nucl-th].
- [29] S. Wang, Y. Z. Jiang, Y. M. Liu, D. Keane, D. Beavis, S. Y. Chu, S. Y. Fung, M. Vient, C. Hartnack, and H. Stoecker, Measurement of collective flow in heavy ion collisions using particle pair correlations, *Phys. Rev. C* **44**, 1091 (1991).
- [30] J. Jiang *et al.*, High order collective flow correlations in heavy ion collisions, *Phys. Rev. Lett.* **68**, 2739 (1992).
- [31] R. S. Bhalerao, M. Luzum, and J.-Y. Ollitrault, Determining initial-state fluctuations from flow measurements in heavy-ion collisions, *Phys. Rev. C* **84**, 034910 (2011), arXiv:1104.4740 [nucl-th].
- [32] N. Borghini, P. M. Dinh, and J.-Y. Ollitrault, New method for measuring azimuthal distributions in nucleus-nucleus collisions, *Phys. Rev. C* **63**, 054906 (2001).
- [33] N. Borghini, P. M. Dinh, and J.-Y. Ollitrault, Flow analysis from multiparticle azimuthal correlations, *Phys. Rev. C* **64**, 054901 (2001).
- [34] A. Bilandzic, C. H. Christensen, K. Gulbrandsen, A. Hansen, and Y. Zhou, Generic framework for anisotropic flow analyses with multiparticle azimuthal correlations, *Phys. Rev. C* **89**, 064904 (2014).
- [35] A. Bilandzic, M. Lesch, C. Mordasini, and S. F. Taghavi, Multivariate cumulants in flow analyses: The next generation, *Phys. Rev. C* **105**, 024912 (2022).

- [36] A. Bilandzic, C. H. Christensen, K. Gulbrandsen, A. Hansen, and Y. Zhou, Generic framework for anisotropic flow analyses with multiparticle azimuthal correlations, *Phys. Rev. C* **89**, 064904 (2014), arXiv:1312.3572 [nucl-ex].
- [37] S. F. Taghavi, A Fourier-cumulant analysis for multiharmonic flow fluctuation: by employing a multidimensional generating function approach, *Eur. Phys. J. C* **81**, 652 (2021), arXiv:2005.04742 [nucl-th].
- [38] J. Adam *et al.* (STAR), Correlation measurements between flow harmonics in au+au collisions at rhic, *Physics Letters B* **783**, 459 (2018).
- [39] J. Adam *et al.* (ALICE), Correlated event-by-event fluctuations of flow harmonics in Pb-Pb collisions at $\sqrt{s_{NN}} = 2.76$ TeV, *Phys. Rev. Lett.* **117**, 182301 (2016), arXiv:1604.07663 [nucl-ex].
- [40] M. Nasim, Systematic study of symmetric cumulants at $\sqrt{s_{NN}} = 200$ GeV in Au+Au collision using transport approach, *Phys. Rev. C* **95**, 034905 (2017), arXiv:1612.01066 [nucl-ex].
- [41] J. E. Parkkila, A. Onnerstad, S. F. Taghavi, C. Mordasini, A. Bilandzic, M. Virta, and D. J. Kim, New constraints for QCD matter from improved Bayesian parameter estimation in heavy-ion collisions at LHC, *Phys. Lett. B* **835**, 137485 (2022), arXiv:2111.08145 [hep-ph].
- [42] C. Mordasini, A. Bilandzic, D. Karakoç, and S. F. Taghavi, Higher order Symmetric Cumulants, *Phys. Rev. C* **102**, 024907 (2020), arXiv:1901.06968 [nucl-ex].
- [43] X. Zhu, Y. Zhou, H. Xu, and H. Song, Correlations of flow harmonics in 2.76A TeV Pb-Pb collisions, *Phys. Rev. C* **95**, 044902 (2017), arXiv:1608.05305 [nucl-th].
- [44] B. Schenke, C. Shen, and P. Tribedy, Multiparticle and charge-dependent azimuthal correlations in heavy-ion collisions at the Relativistic Heavy-Ion Collider, *Phys. Rev. C* **99**, 044908 (2019), arXiv:1901.04378 [nucl-th].
- [45] H. Hirvonen, K. J. Eskola, and H. Niemi, Flow correlations from a hydrodynamics model with dynamical freeze-out and initial conditions based on perturbative QCD and saturation, *Phys. Rev. C* **106**, 044913 (2022), arXiv:2206.15207 [hep-ph].
- [46] N. Magdy, Characterizing initial- and final-state effects of relativistic nuclear collisions, *Phys. Rev. C* **107**, 024905 (2023), arXiv:2210.14091 [nucl-th].
- [47] N. Magdy, Characterizing the initial- and final-state effects in isobaric collisions at energies available at the BNL Relativistic Heavy Ion Collider, *Phys. Rev. C* **109**, 024906 (2024), arXiv:2401.04083 [nucl-th].
- [48] F. G. Gardim, F. Grassi, M. Luzum, and J. Noronha-Hostler, Hydrodynamic Predictions for Mixed Harmonic Correlations in 200 GeV Au+Au Collisions, *Phys. Rev. C* **95**, 034901 (2017), arXiv:1608.02982 [nucl-th].
- [49] S. Acharya *et al.* (ALICE), Systematic studies of correlations between different order flow harmonics in Pb-Pb collisions at $\sqrt{s_{NN}} = 2.76$ TeV, *Phys. Rev. C* **97**, 024906 (2018), arXiv:1709.01127 [nucl-ex].
- [50] S. Acharya *et al.* (ALICE), Higher-order correlations between different moments of two flow amplitudes in Pb-Pb collisions at $\sqrt{s_{NN}} = 5.02$ TeV, *Phys. Rev. C* **108**, 055203 (2023), arXiv:2303.13414 [nucl-ex].
- [51] M. Aaboud *et al.* (ATLAS), Correlated long-range mixed-harmonic fluctuations measured in *pp*, *p+Pb* and low-multiplicity Pb+Pb collisions with the ATLAS detector, *Phys. Lett. B* **789**, 444 (2019), arXiv:1807.02012 [nucl-ex].
- [52] A. Ortiz (ALICE, ATLAS, CMS, LHCb), Particle production and flow-like effects in small systems, *PoS LHCP2019*, 091 (2019), arXiv:1909.03937 [hep-ex].
- [53] A. M. Sirunyan *et al.* (CMS), Correlations of azimuthal anisotropy Fourier harmonics with subevent cumulants in *pPb* collisions at $\sqrt{s_{NN}} = 8.16$ TeV, *Phys. Rev. C* **103**, 014902 (2021), arXiv:1905.09935 [hep-ex].
- [54] S. Acharya *et al.* (ALICE), Measurements of mixed harmonic cumulants in Pb-Pb collisions at $\sqrt{s_{NN}} = 5.02$ TeV, *Phys. Lett. B* **818**, 136354 (2021), arXiv:2102.12180 [nucl-ex].
- [55] Q. Y. Shou, Y. G. Ma, P. Sorensen, A. H. Tang, F. Videbæk, and H. Wang, Parameterization of Deformed Nuclei for Glauber Modeling in Relativistic Heavy Ion Collisions, *Phys. Lett. B* **749**, 215 (2015), arXiv:1409.8375 [nucl-th].
- [56] B. Schenke, S. Jeon, and C. Gale, (3+1)D hydrodynamic simulation of relativistic heavy-ion collisions, *Phys. Rev. C* **82**, 014903 (2010), arXiv:1004.1408 [hep-ph].
- [57] B. Schenke, S. Jeon, and C. Gale, Elliptic and triangular flow in event-by-event (3+1)D viscous hydrodynamics, *Phys. Rev. Lett.* **106**, 042301 (2011), arXiv:1009.3244 [hep-ph].
- [58] J.-F. Paquet, C. Shen, G. S. Denicol, M. Luzum, B. Schenke, S. Jeon, and C. Gale, Production of photons in relativistic heavy-ion collisions, *Phys. Rev. C* **93**, 044906 (2016), arXiv:1509.06738 [hep-ph].
- [59] P. Huovinen and H. Petersen, Particlization in hybrid models, *Eur. Phys. J. A* **48**, 171 (2012), arXiv:1206.3371 [nucl-th].
- [60] G. S. Denicol, T. Kodama, T. Koide, and P. Mota, Bulk viscosity effects on elliptic flow, *Nucl. Phys. A* **830**, 729C (2009), arXiv:0907.4269 [hep-ph].
- [61] A. Monnai, B. Schenke, and C. Shen, Equation of state at finite densities for QCD matter in nuclear collisions, *Phys. Rev. C* **100**, 024907 (2019), arXiv:1902.05095 [nucl-th].
- [62] A. Bazavov *et al.* (HotQCD), Equation of state in (2+1)-flavor QCD, *Phys. Rev. D* **90**, 094503 (2014), arXiv:1407.6387 [hep-lat].
- [63] A. Bazavov *et al.* (HotQCD), Fluctuations and Correlations of net baryon number, electric charge, and strangeness: A comparison of lattice QCD results with the hadron resonance gas model, *Phys. Rev. D* **86**, 034509 (2012), arXiv:1203.0784 [hep-lat].
- [64] H. T. Ding, S. Mukherjee, H. Ohno, P. Petreczky, and H. P. Schadler, Diagonal and off-diagonal quark number susceptibilities at high

- temperatures, Phys. Rev. D **92**, 074043 (2015), arXiv:1507.06637 [hep-lat].
- [65] J. S. Moreland and R. A. Soltz, Hydrodynamic simulations of relativistic heavy-ion collisions with different lattice quantum chromodynamics calculations of the equation of state, Phys. Rev. C **93**, 044913 (2016), arXiv:1512.02189 [nucl-th].
- [66] C. Shen, Z. Qiu, H. Song, J. Bernhard, S. Bass, and U. Heinz, The iEBE-VISHNU code package for relativistic heavy-ion collisions, Comput. Phys. Commun. **199**, 61 (2016), arXiv:1409.8164 [nucl-th].
- [67] The iSS code package can be downloaded from GitHub.
- [68] M. Bleicher *et al.*, Relativistic hadron hadron collisions in the ultrarelativistic quantum molecular dynamics model, J. Phys. G **25**, 1859 (1999), arXiv:hep-ph/9909407.
- [69] S. A. Bass *et al.*, Microscopic models for ultrarelativistic heavy ion collisions, Prog. Part. Nucl. Phys. **41**, 255 (1998), arXiv:nucl-th/9803035.
- [70] B. I. Abelev *et al.* (STAR), Systematic Measurements of Identified Particle Spectra in pp, d^+ Au and Au+Au Collisions from STAR, Phys. Rev. C **79**, 034909 (2009), arXiv:0808.2041 [nucl-ex].
- [71] A. Adare *et al.* (PHENIX), Measurements of Higher-Order Flow Harmonics in Au+Au Collisions at $\sqrt{s_{NN}} = 200$ GeV, Phys. Rev. Lett. **107**, 252301 (2011), arXiv:1105.3928 [nucl-ex].
- [72] B. Schenke, S. Jeon, and C. Gale, Higher flow harmonics from (3+1)D event-by-event viscous hydrodynamics, Phys. Rev. C **85**, 024901 (2012), arXiv:1109.6289 [hep-ph].
- [73] J. Adam *et al.* (STAR), Correlation Measurements Between Flow Harmonics in Au+Au Collisions at RHIC, Phys. Lett. B **783**, 459 (2018), arXiv:1803.03876 [nucl-ex].
- [74] D. Teaney and L. Yan, Non linearities in the harmonic spectrum of heavy ion collisions with ideal and viscous hydrodynamics, Phys. Rev. C **86**, 044908 (2012), arXiv:1206.1905 [nucl-th].
- [75] G. Aad *et al.* (ATLAS), Measurement of the correlation between flow harmonics of different order in lead-lead collisions at $\sqrt{s_{NN}}=2.76$ TeV with the ATLAS detector, Phys. Rev. C **92**, 034903 (2015), arXiv:1504.01289 [hep-ex].

F. Appendix

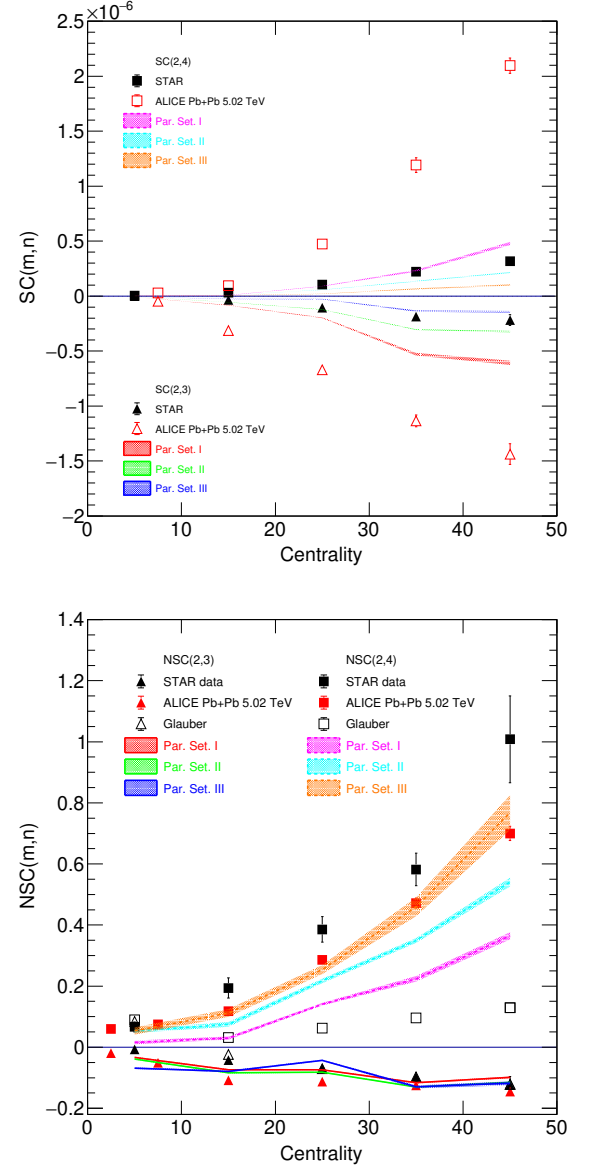


FIG. 7. (Normalized) Symmetric cumulant vs centrality from four-particle correlations in Au+Au collisions at $\sqrt{s_{NN}} = 200$ GeV compared with ALICE measurements for Pb+Pb 5.02 TeV [50, 54].

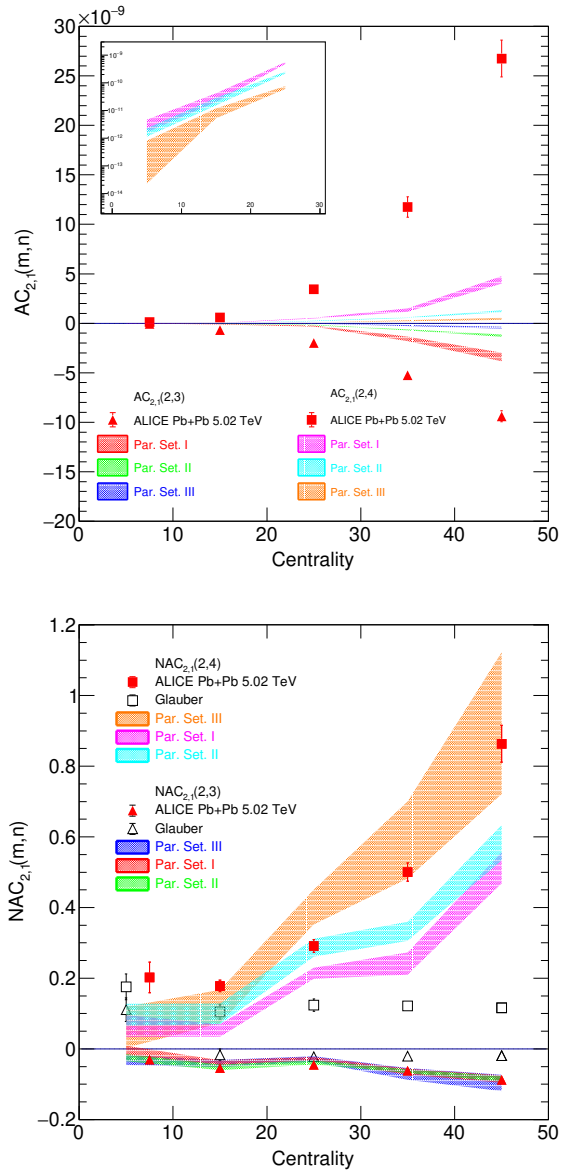


FIG. 8. (Normalized) Asymmetric cumulant vs centrality from six-particle correlations in Au+Au collisions at $\sqrt{s_{NN}} = 200$ GeV compared with ALICE measurements for Pb+Pb 5.02 TeV [50, 54].